Spatiotemporal properties of solitons excited on the surface of shallow water in a hydrodynamic resonator

Alexander Ezersky, O. Polukhina, Jérôme Brossard, François Marin, Innocent Mutabazi

Spatiotemporal properties of solitons excited on the surface of shallow water in a hydrodynamic resonator

A. B. Ezersky and O. E. Polukhina
Institute of Applied Physics, 46 Ulyanov Street, 603950 Nizny Novogorod, Russia

J. Brossard, F. Marin, and I. Mutabazi[a)]
Laboratoire de Mécanique, Physique et Géosciences, Université du Havre, B.P. 540, 76058 Le Havre Cedex, France

(Received 31 July 2005; accepted 11 April 2006)

We have investigated the spatiotemporal properties of solitons generated on the shallow water surface over a background of a large-scale mode in a hydrodynamic resonator when it is forced near the second frequency mode. We have used the space-time diagrams to highlight the spatiotemporal dynamics of nonlinear fields for two solitons colliding in a resonator and compared them to those of solitons occurring in an unbounded system. A state diagram of experimentally observed modes for different values of the excitation parameters has been obtained. In particular, we have evidenced period doubling and the multistability of nonlinear waves excited in the resonator. For a theoretical description of these experimental results, we have developed a phenomenological model, which leads to amplitude and phase equations of a soliton propagating over the background of a harmonic wave. To reproduce experimental results on the multistability, we have supplemented our analysis with a numerical simulation of a modified system of Boussinesq equations for shallow water, taking into account the dissipation effect © *2006 American Institute of Physics*. [DOI: 10.1063/1.2204968]

I. INTRODUCTION

Solitons observed in many systems such as the shallow water channel in nonlinear electrical lines or in protein chains, exhibit astonishing stability properties, the investigation of which remains a very active research area.[1,2] The excitation of solitons on the surface of shallow water and their dynamics have been addressed mostly for infinitely extended systems.[1,2] In an unbounded medium, solitons arising from an initial perturbation propagate in opposite directions and diverge in a finite time, hence their interaction can be neglected. Therefore, the main attention of the researchers was focused on the behavior of the solitons propagating in one direction. Experimentally, such solitons were excited by a single displacement of a piston pushing the liquid in the horizontal direction[3,4] or by producing an initial elevation in the level of liquid in a finite region.[5,6] The dynamics of such solitons is described by the well-known Korteweg-de Vries (KdV) equation that is derived under the assumption of wave propagation in one direction. Feng[7] investigated traveling solitary wave solutions in the Boussinesq equations, which describe counterpropagating waves, but he presented only waves propagating in one direction. Besides the generation of a soliton or a sequence of solitons of surface waves from initial perturbations,[8] individual properties of interaction have been investigated thoroughly, namely, the interaction of two solitons, the reflection of a soliton at a vertical wall,[3,9] an uneven bottom,[10] and so on. It was found, in particular, that the soliton amplitude at the instant of reflection at the wall increases more than twice, and the reflected soliton lags behind the time calculated under the assumption of the constant velocity of soliton propagation.[9] When two solitons interact, similar effects are observed: the time lag and the amplitude of surface displacement larger than the sum of the individual soliton amplitudes. It is worthy of notice that the majority of experiments agree well with basic assumptions of the theory;[11–14] specifically, solitons come from one infinity, interact with a wall or with each other, and go to the opposite infinity.[15] However, solitons can be excited, not only in systems of infinite length, but in resonators too. One expects that the spatiotemporal dynamics of solitons will be different in resonators, where the interaction of nonlinear waves propagating in opposite directions can no longer be neglected. Experimental works on surface wave solitons in resonators are rather scanty. The parametric excitation of nonlinear waves, including soliton-like pulses, was described in Refs. 16 and 17 for experiments in a 60 cm long cuvette, performing horizontal oscillations. That work was published 38 years ago, when the properties of solitons and even the term ≪soliton≫ itself were not known to the broad public. The authors of Refs. 16 and 17 called the observed waves ≪resonant oscillations≫, as they were excited near the first resonant frequency of the tank. They studied the time series of free surface displacements at several points of a resonator and did not present any information about the spatiotemporal dynamics of the perturbations. This work has stimulated a large number of theoretical and numerical studies on solitons, most of which were concerned with asymptotic methods applied to the Korteveg-de Vries equation, with forcing near the fundamental[18–20] or half the fundamental frequency.[21] Modes of the parametric excitation of one or several nonpropagating oscillating solitons were described in

[a)]Author to whom correspondence should be addressed. Electronic mail: innocent.mutabazi@univ-lehavre.fr

Ref. 22, where it was found that the displacement amplitude of the free surface in such nonlinear waves is close to the classical soliton, with the fields decreasing exponentially at large distances. Soliton excitation in wave resonators has been performed in systems whose physical nature is absolutely different from that of surface waves, but that, nevertheless, possess similar dispersive and nonlinear characteristics as surface waves on shallow water. For instance, solitons of electromagnetic waves were observed on a section of an LC line excited by sinusoidal voltage,[23] and solitons of transverse waves were observed in a rubber strip at parametric excitation by a harmonic external force.[24]

When solitons are excited in resonators, we face problems that are quite different from those in spatially infinite systems, because of the multiple interactions of solitons propagating in a resonator, as well as the interaction between solitons and resonator modes. In this paper, we have investigated these phenomena excited near the second resonant frequency of a hydrodynamic resonator of a larger length. We have determined a state diagram of different excited modes. We have used the space-time diagrams technique that allows for a better visualization of spatiotemporal properties of wave phenomena and a better comparison between experimental and numerical results. In particular, we have thoroughly characterized the soliton collision by measuring residence time and merging length. We have evidenced the existence of soliton bound state generation. In order to reproduce some states observed in experiments, we have solved numerically the Boussinesq equations with dissipation terms.

The paper is organized as follows. The experimental procedure on soliton excitation in a water wave resonator is described in Sec. II. Results are presented in Sec. III, where, in particular, a state diagram is presented in the space of the excitation parameters (amplitude and frequency). In Sec. IV we compare some of our experimental results with those obtained in experiments on soliton reflection from a vertical wall carried out by Maxworthy.[3] We introduce a simplified model for the amplitude and phase of the soliton interacting with the monochromatic wave. The section ends with the presentation of a numerical solution of a modified system of the Boussinesq equations for shallow water waves. In Sec. V we draw some concluding remarks.

II. EXPERIMENTAL SETUP

The experiment was carried out in a water tank of length $L=10$ m and width $D=0.5$ m, with a liquid depth $H=0.26$ m. Hence, the ratio $\mu=H/L=0.026<<1$ lies in the allowed range of the shallow water approximation.[2] Surface waves were excited by a wavemaker (Fig. 1), which consists of a flat plate driven into a periodic motion by an electric motor. The plate rotated around the point O_1 (Fig. 1), the amplitude of its horizontal displacement, depends on depth; that is why we have used the average value of this amplitude, defined as

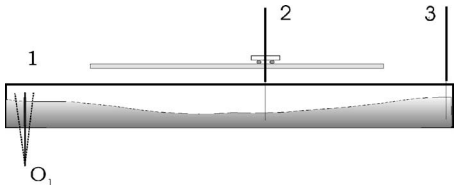

FIG. 1. Experimental setup: 1 – wave maker, O_1 – the rotation axis of a flat plate; 2 – movable resistive sensor; 3 – stationary resistive sensor.

$$a_{ex}=\frac{1}{H}\int_0^H a(z)dz. \tag{136}$$

Displacement of the free surface was measured by two resistance-wire wave gauges (Fig. 1). One of them was moved at distances up to 5.6 m in the central part of the tank, while the second one was fixed at the wall reflecting the surface waves. The hydrodynamic resonator has eigenmodes with frequencies given in Ref. 25:

$$f_n=\frac{1}{2\pi}\sqrt{gk_n\tanh z(k_nH)}, \tag{143}$$

where g is the gravity acceleration and $k_n=n\pi/L, n=1,2,3,\ldots$. For shallow water $k_nH<<1$ and the frequency becomes $f_n\approx k_n\sqrt{gH}$. The frequency of the wavemaker in the experiment was chosen to be close to that of the mode whose wavelength was equal to the resonator length $\lambda=L$, i.e., $n=2$ and $f_2\approx L^{-1}\sqrt{gh}$, which gives for our resonator dimensions $f_2=0.1645$ Hz. At this frequency, standing harmonic surface waves of maximal amplitude were excited in the resonator at a very small amplitude of external forcing. When the external force frequency was detuned by a small value from f_2, the amplitude of the standing waves in the resonator decreased. We measured the mismatch from exact resonance $\delta f_2=f_{ex}-f_2$ at which the amplitude of oscillations in the resonator decreased by $\sqrt{2}$ times. We have found that this mode had a rather high Q factor (defined as $Q=f_2/\delta f_2\geq 50$) induced by the dissipation in the system. The value $Q=50$ means that the mode oscillations at frequency f_2 damp $e=2.71\ldots$times over 50 periods, or approximately during 5 min. The hydrodynamic resonator has two main control parameters: the average excitation amplitude a_{ex} and the excitation frequency f_{ex} (or the detuning parameter δf_2).

III. RESULTS

A. Space-time diagrams

Signals from the two sensors were used to construct space-time diagrams. We registered the time series at 56 points by moving the sensor along the channel and, simultaneously, registered the signal from the stationary sensor for each of these points. The signal from the stationary sensor was used as a reference signal, and phase averaging was made. This procedure of constructing space-time diagrams is valid for regimes that are strictly periodic in time. If the regime has no time period, many sensors may be needed from which signals must be registered simultaneously. Space-time diagrams obtained in an experiment depend significantly on the control parameters a_{ex} and δf_2.

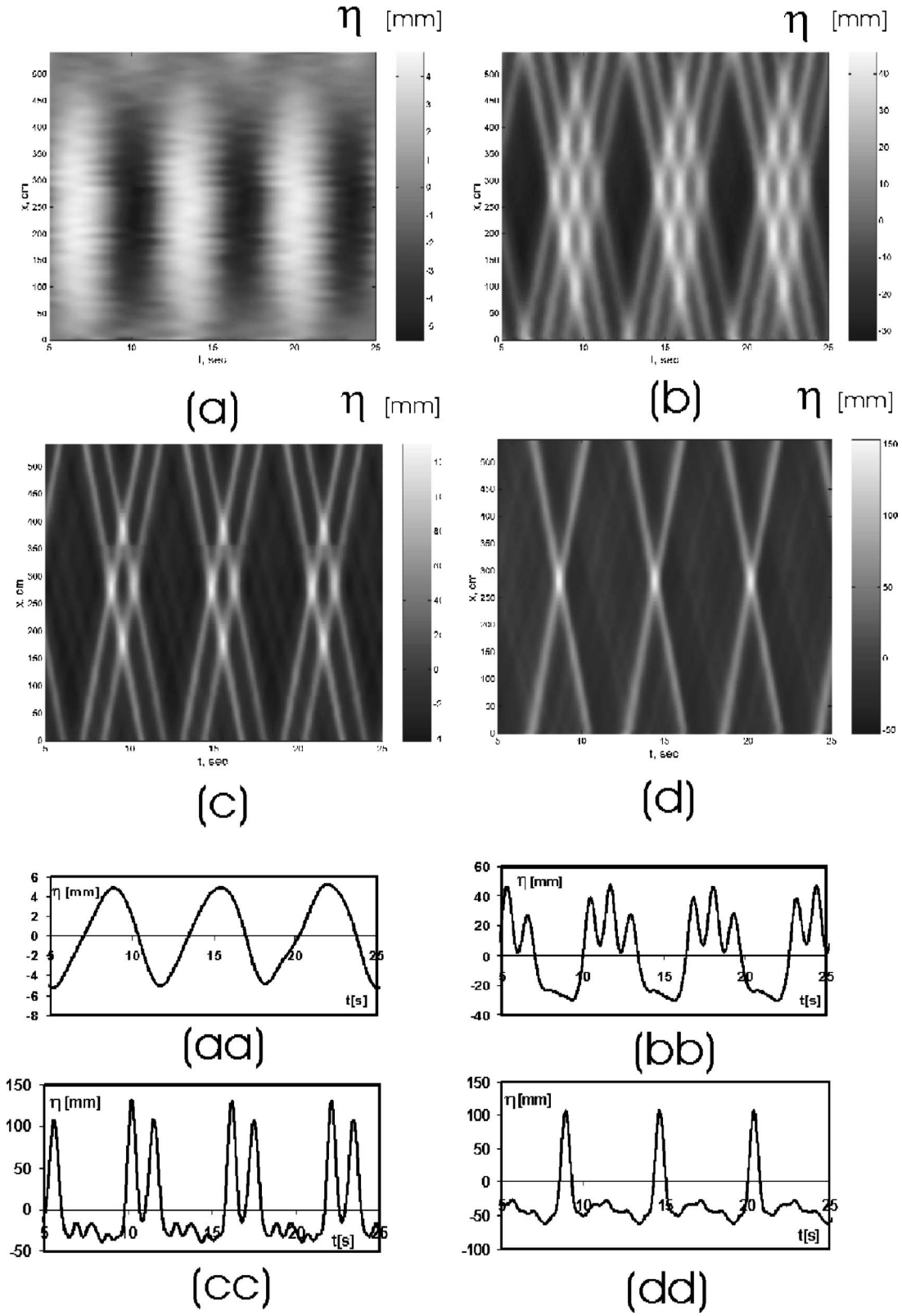

FIG. 2. Space-time diagrams and time series from stationary sensor: (*a*), (*aa*) a_{ex}=2.3 cm, f_{ex}=0.151 Hz, $Q^{-1}=(f_{ex}-f_2)/f_2=-0.087$; (b), (bb) a_{ex}=8.2 cm, f_{ex}=0.158 Hz, $Q^{-1}=-0.045$; (c), (cc) a_{ex}=8.2 cm, f_{ex}=0.170 Hz, $Q^{-1}=0.028$; (d), (dd) a_{ex}=8.2 cm, f_{ex}=0.177 Hz, $Q^{-1}=0.07$.

Typical diagrams for different parameters of external forcing, as well as the time series obtained by means of the stationary sensor located at the wall, are given in Fig. 2. It is clear from these diagrams that, for a small amplitude of the external forcing, standing surface waves are excited in the resonator [Fig. 2(a)], which correspond to the time series (aa). For larger amplitudes, propagating pulses arise in the system [Figs. 2(b)–2(d)] and the time series are seen in (bb)–

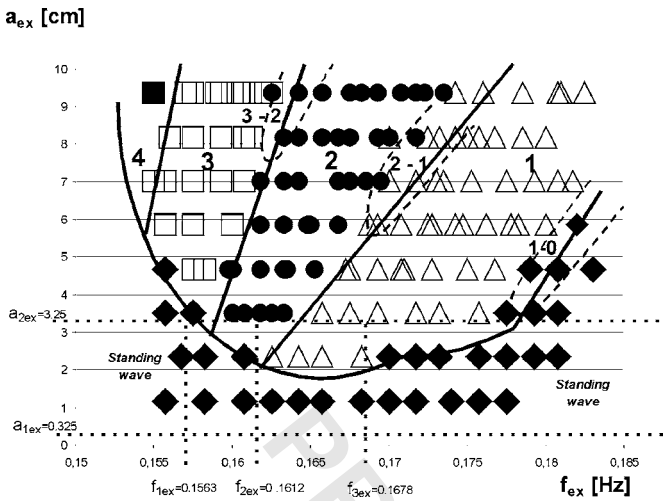

FIG. 3. Partitioning of the (f_{ex}, a_{ex}) plane into regions with different regimes of generation of nonlinear waves. Numbers 1, 2, 3, 4 mean the number of impulses generated on the background of the time period of harmonic wave. Regions isolated by the dashed curves correspond to the parameters under which generation regimes (generation of 3 or 2, 2 or 1, 1 or 0 impulses) depend on the initial conditions.

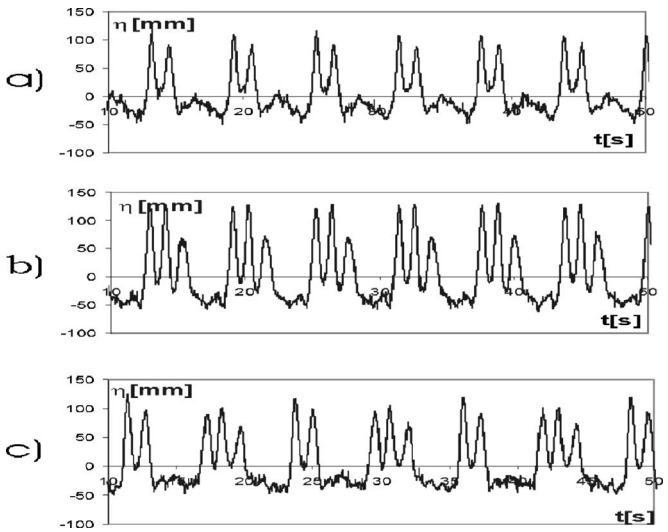

FIG. 4. Multistability observed at $a_{ex}=9.4$ cm, $f_{ex}=0.165$ Hz (region *2-3* in Fig. 3).

(dd). The pulses are visualized as bright strips in the space-time diagrams. The pulse propagation velocity given by the slope of the strips was close to the velocity of surface waves on shallow water in our experimental conditions. If we represent a standing wave as a superposition of two traveling waves propagating in opposite directions, pulses propagate synchronously with each of these waves. The number of pulses (from 1 to 4 in most of our experiments) registered by a sensor is different at different points of the resonator, and it coincides with the number of pulses for each traveling wave only in the center of the resonator and near its side boundaries. The number of pulses depends on the excitation frequency and on the amplitude. For a frequency lower than the resonance frequency of the mode, three pulses are excited on the wave period. Two intersecting triples of such tracks are illustrated in Fig. 2(b). For the excitation frequency higher than the resonance frequency, only one pulse arises, hence, two intersecting tracks only are seen in Fig. 2(d).

In Fig. 3 we have represented the t wave states of qualitatively different dynamics in the plane of parameters (f_{ex}, a_{ex}). The labels 1, 2, 3, or 4 in the regions of the state diagram indicate the number of pulses excited on the wave period. When the amplitude is large enough, there exists a small region where four pulses can be excited. For the control parameters within the zones marked by a dashed line, multistability is observed, i.e., different regimes may occur at the same values of frequency and wavemaker oscillation amplitude, but under different initial conditions. For example, the excitation of two [Fig. 4(a)] or three [Fig. 4(b)] pulses, or the alternate generation of two or three pulses on a period [Fig. 4(c)]) occur in zones 2–3. The regime in Fig. 4(c) corresponds to period doubling: nonlinear waves excited in the system have a period twice as large as the period of wavemaker oscillations.

B. Extraction of solitons

A detailed analysis of the experimental data revealed that, within a definite interval of control parameters, characteristics of the pulses excited in the resonator are close to those of solitons. To verify this statement, we have assumed that pulses in the resonator are excited against the background of a harmonic wave. The problem is how to separate pulses and harmonic oscillations. Obviously, this cannot be done by linear filters, as the repetition rate of pulses is equal exactly to the frequency of harmonic oscillations. Consequently, we determined the position of pulse maxima [Fig. 5(a)], and then the resulting data were replaced in the interval $\tau_1+\tau_2$ by the linear dependence of the free surface displacement on time. In this fashion we were able to separate the pulses. Further, all the harmonics with the frequency larger than the excitation frequency were separated from the obtained signal by filtering. The resulting signal as well as the initial time series are depicted in Fig. 5(b). Figure 5(c) illustrates separately the harmonic mode of the resonator and the sequence of pulses. Apparently, the results of filtering depend significantly on the way we choose τ_1 and τ_2. Different trials for quantities τ_1 and τ_2 showed that, with a reasonable choice of these parameters ($\tau_{1,2}<T/6$, where T is the period of external force), the scatter in the characteristics of harmonic oscillations and pulses is insignificant. Following this algorithm the time series were processed by the LabView 4.1 software. It was revealed that the shape of the pulses is close to classical solitons: $A=A_s\cosh^{-2}(t/\tau_s)$ (A_s stands for the amplitude of the soliton), everywhere except in regions where the field amplitude is small, for instance, in the oscillating tails of solitons (Fig. 6). The pulse duration τ_s defined at the level $A/A_s=\cosh^{-2}(1)/0.4199$, as a function of the pulse amplitude, is plotted in Fig. 7. We found that the pulse duration decreases with the increasing amplitude of the pulse, A_s. Pulses observed in the experiment are localized in a finite region of space and their characteristics are close to those of the theoretical soliton; therefore we have called them *solitons*.

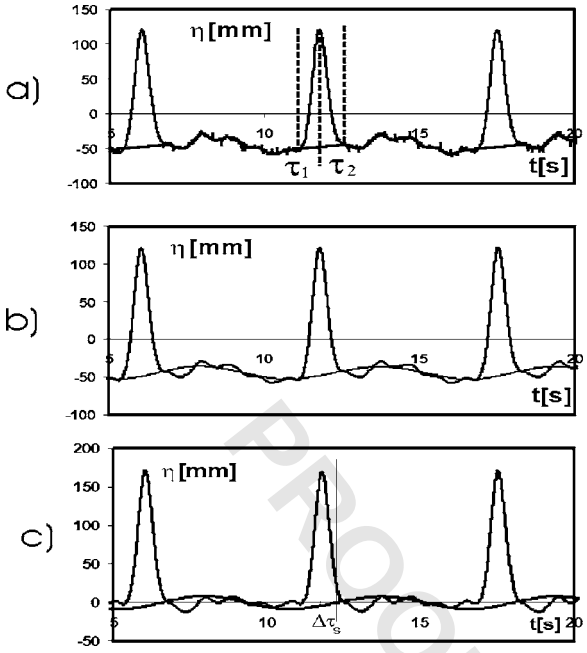

FIG. 5. Extraction of solitons and harmonic wave from the time series: (a) initial time series and series with solitons cut off on the interval $\tau_1+\tau_2$; (b) harmonic wave and "harmonic wave+soliton;" (c) a sequence of solitons and harmonic wave. The phase shift of soliton and harmonic wave $\varphi_s = \Delta\tau_s\,\omega$, where $\omega = 2\pi f_{ex}$.

C. Properties of the observed solitons

The extraction of solitons and a harmonic wave from a time series allows one to compare the properties of nonlinear waves observed in the experiment with the well-known solutions of the Korteweg-de Vries (KdV) equation (2) that governs the displacement of free surface of shallow water:

$$\frac{\partial \eta}{\partial t} + V_0\frac{\partial \eta}{\partial x} + \frac{3}{2}\frac{V_0}{H}\eta\frac{\partial \eta}{\partial x} + \frac{1}{6}V_0H^2\frac{\partial^3 \eta}{\partial x^3} = 0, \qquad (1)$$

where $V_0=\sqrt{gH}$ is the velocity of surface waves of infinitely small amplitude in shallow water. The KdV equation has solutions in the form of a soliton[2]:

$$\eta_s(x - V_st) = A_s\cosh^{-2}\left(\sqrt{\frac{3A_s}{4H^3}}(x - V_st)\right),$$

$$V_s = V_0\left(1 + \frac{A_s}{2H}\right). \qquad (2)$$

Clearly, the duration of the soliton is proportional to $A_s^{-1/2}$ (the solid line in Fig. 7); its velocity depends linearly on its amplitude A_s, and the soliton size decreases with an increase of its amplitude.

In order to measure the phase shift between the soliton and background wave, we have assumed that nonlinear waves excited in a resonator consist of two solitons propagating toward each other, and each of them is propagating against the background of a harmonic wave. We have neglected the interaction of counterpropagating waves and represented the nonlinear field of surface displacement as a superposition of four components:

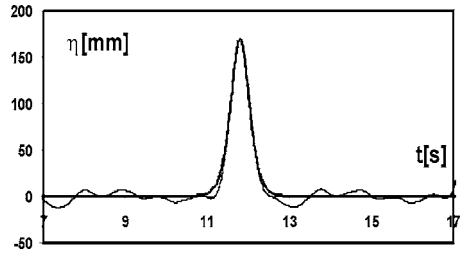

FIG. 6. A comparison of the shape of pulse with the theoretical dependence $\eta=A_s\cosh^{-2}[(t-t_0)/\tau_s]$, where $t_0=x/V_s$.

$$\eta(t,x) = \eta_s(x - V_st) + \eta_0\sin(\omega t - kx - \varphi_s) + \eta_s(x + V_st) + \eta_0\sin(\omega t + kx - \varphi_s), \qquad (3)$$

where ω, k are the frequency and wavenumber of harmonic waves, η_0 is the wave amplitude, and φ_s is the phase shift between the soliton and the harmonic wave [Fig. 5(c)]. Near the reflecting endwall ($x=0$), where the stationary sensor is located, the displacement of the free surface can be represented in the form

$$\eta = 2\eta_0\sin(\omega t - \varphi_s) + 2\eta_s(t).$$

This relation allows for a comparison of our experimental results with analytical theory for the soliton-harmonics interaction developed in Ref. 23 and, in particular, for measuring the phase shift φ_s. The results of the measuring phase shift φ_s are presented in Fig. 8. For a small amplitude of external force, the phase shift was close to zero. As the amplitude increased, the phase shift increased up to 40°–60°. The amplitude of the soliton depended on the frequency and amplitude of the wavemaker. For the same amplitude of external forcing, the soliton amplitude and phase depended on the frequency of the external force. By measuring the time at which the soliton amplitude reaches its maximum at different positions of a sensor of free surface displacement, we have determined the trajectory of soliton motion (Fig. 9). From these trajectories, we have measured the velocity of soliton motion on different sections of the trajectory, except in the region of the merging of two maxima. A linear fit of the data

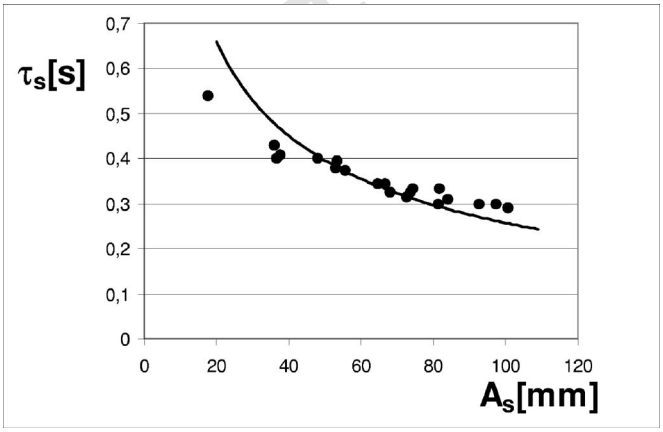

FIG. 7. The soliton duration *versus* the soliton amplitude as obtained in experiment (dots). The theoretical dependence $\tau_s=(1/V_s)\sqrt{4H^3/3A_s}$, where $V_s=V_0(1+A_s/2H)$ is also plotted for comparison (curve).

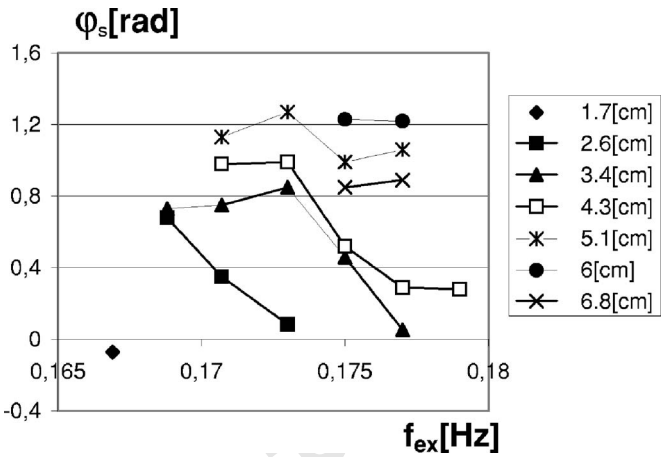

FIG. 8. The soliton phase φ_s *versus* the external force frequency f_{ex}. Data for different external force amplitudes a_{ex} are marked by different symbols.

showed that the soliton has approximately constant velocity $V_s \approx f_{ex}L$ on all the sections. The solitons propagate synchronously with the harmonic wave.

The space-time diagrams illustrate how in the central part of the resonator solitons propagating in opposite directions collide and merge. The size L_m of the merging region depends on the pulse amplitude, as is clearly seen in Fig. 10. The larger is the pulse amplitude, the less extended is the region of merging. The pulse interaction leads to a significant change in their velocity.

IV. DISCUSSION OF RESULTS

A. Merging length and residence time

The method of characteristics has been used by Maxworthy[3] to investigate the soliton interaction with a wall; we may compare our results on soliton interaction in resonators with his results. Maxworthy showed that the collision of two counterpropagating surface wave solitons of equal amplitude in an unbounded medium is equivalent to the reflection of one soliton from a vertical wall. Indeed, on reflection from a vertical wall, the horizontal velocity of perturbations is zero, and when two solitons of the same amplitude collide there is a symmetry axis along which the horizontal velocity is also zero. Maxworthy made a film in his experiment and processed its individual shots—instantaneous snapshots of surface elevation from which he constructed soliton trajectories. In our experiments we constructed an (X-T) diagram using a time series of surface displacement measured at different points. These are, actually, diagram sections at a fixed coordinate. Thus, the two problems are identical. By calculating the position of the maximum of surface displacement for each section, one can construct a trajectory of soliton motion. An example of such a trajectory is given in Fig. 9(a). The arrows show the direction of soliton motion. The best linear fit of the points is shown for different parts of the trajectories. Velocities of the solitons are different in the four parts. Our diagrams can also be used to determine a trajectory like it was done by Maxworthy. Toward this end, one must determine in the (X-T) diagram sections at fixed moments of time. Note that a trajectory will be different if one

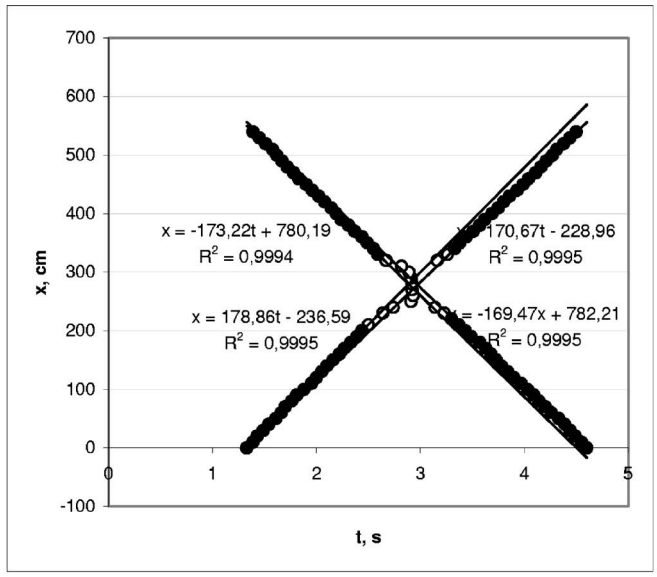

a)

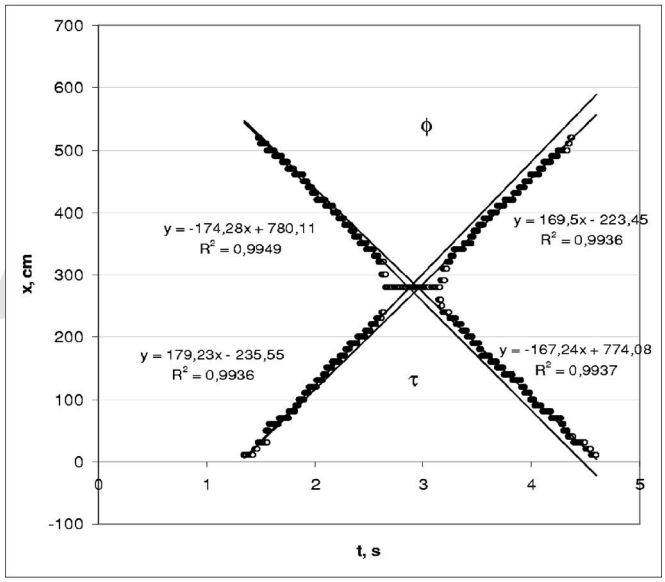

b)

FIG. 9. Soliton trajectories in a resonator for a_{ex}=8.2 cm, f_{ex}=0.177 Hz. Arrows indicate directions of soliton propagation. (a) Soliton trajectories determined by snapshots; (b) soliton trajectories determined by time series; ϕ is the soliton lag.

first finds sections at a fixed time and then calculates the position of the maximum along the coordinate [Fig. 9(b)]. In the first case [Fig. 9(a)], there exists a length L_m that can be referred to as the merging length. In the second case, there is time τ, which is referred to as residence time [Fig. 9(b)] during which the maximum stays at one point. The residence time was determined for different amplitudes of colliding solitons. For example, for the case depicted in Fig. 9(b), the dimensionless residence time is $\tau' = \tau\sqrt{g/H} = 2.9$ for the dimensionless soliton amplitude $\varepsilon = A_s/H = 0.28$. These values are in good agreement with the data obtained by Cooker *et al.*[9] from Maxworthy's film,[3] as well as with the results of numerical calculations also reported in Ref. 9. For instance, numerical calculations[9] give $\tau = 3.2$ for $\varepsilon = 0.28$, which al-

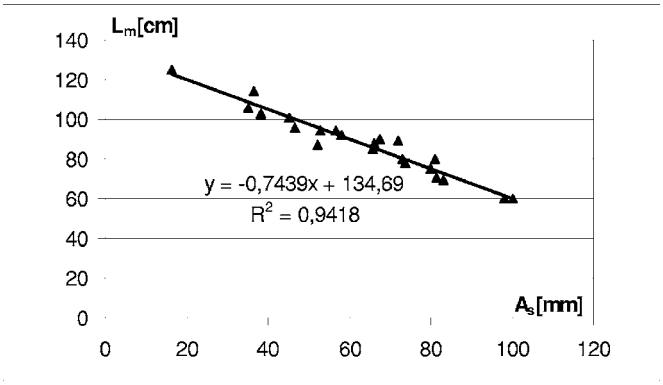

FIG. 10. The merging length L_m *versus* the soliton amplitude A_s.

most coincides with the data of Maxworthy's film. For smaller amplitudes of colliding solitons, the agreement of our results with data of the works[3,9] is worse. This is evidently caused by the influence of monochromatic resonator modes on the collision of small-amplitude solitons in our experiments. Measurements at different amplitudes of external force showed that the difference between soliton velocities before and after collision increases with increasing soliton amplitude.

Maxworthy[3] noted that the amplitude of a soliton reflected from a wall is slightly smaller than before reflection, and attributed this difference to dissipation. When solitons are excited in a resonator, in addition to dissipation, the soliton interaction with a monochromatic mode occurs, and this may lead to an increase in the soliton amplitude. Consequently, for experiments in a resonator, we cannot state that the soliton amplitude before an interaction must be larger than after it. In addition to the effect of velocity change on a soliton collision, we have revealed a small phase shift, soliton lag ϕ caused by their interaction [Fig. 9(b)]. Such a time lag when solitons were reflected at the wall was also reported by Maxworthy.[3]

B. Analytical model of soliton generation

In this section we have compared the characteristics of surface wave solitons measured in the experiment and the results of semiphenomenological theory. A theoretical investigation of nonlinear fields excited by the harmonic force in a resonator was developed for surface waves on shallow water by Chester[17] and for electromagnetic waves in LC lines by Gorshkov *et al.*,[23] where perturbations propagating in resonators were represented as a sum of monochromatic waves and nonlinear perturbations. As the paper[17] appeared before intense investigations into solitons in different fields of science, it did not contain any reference to solitons; however, Gorshkov *et al.*[23] postulated the existence of a soliton on the background of a monochromatic wave. For a description of solitons of electromagnetic waves Gorshkov *et al.* derived equations for the amplitude and the phase of a soliton propagating in a resonator against the background of a monochromatic wave. We have established analogous equations for surface waves on shallow water, and they are written in the form

$$\frac{dE_s}{dt} = \frac{3}{2}\frac{\omega\eta_0}{H}E_s\cos\varphi_s - \alpha E_s, \tag{4a}$$

$$\frac{d\varphi_s}{dt} = \frac{kV_0}{2H}[A_s - 3\eta_0\sin\varphi_s] - \Delta. \tag{4b}$$

Here, E_s stands for soliton energy,

$$E_s = \int_{-\infty}^{\infty}\eta_s^2 dx \approx A_s^2\Delta x_s \propto A_s^{3/2},$$

Δx_s is the width of the soliton, φ_s is the soliton phase that can be understood as the dimensionless time between the maximum of the soliton and the zero of the monochromatic mode [Fig. 5(c)], $\Delta = 2\pi\delta f_2$ is the frequency mismatch, and α is the coefficient describing the exponential damping of the soliton. The first equation in the system (4) is the equation of energy balance. Changes in the soliton amplitude are due to energy transfer from a harmonic wave [the first term in (4); its detailed derivation can be found in the Appendix] and to energy dissipation [the second term in (4a)]. It is worthy of notice that the coefficient α describes a type of dissipation that is independent of the scale of the perturbations. Such dissipation, indeed, is observed in different systems such as the ones considered in Refs. 26 and 27. However, in contrast to other parameters entering the system (4), we did not determine this parameter in our experiment, and in what follows we have chosen it from the requirement that the theoretically predicted parameters of solitons should be as close as possible to the experimental data. The second equation in (4) is a kinematic condition. The soliton velocity in the reference system moving with the velocity of the harmonic wave ($V_{phh} = \omega/k$) depends on the soliton amplitude A_s [the first term in (4b)]. The harmonic wave transports the soliton as a particle with corresponding velocity $u = -\sqrt{g/H}\eta_0\sin\varphi_s$, depending on its phase. As the soliton is superposed on the background of the surface displacement of the harmonic wave, the latter modifies the velocity of soliton propagation by $\Delta V_s = \sqrt{g(H-\eta_0\sin\varphi_s)} - \sqrt{gH} \approx -(1/2)\sqrt{g/H}\eta_0\sin\varphi_s$. The total contribution of these two effects $(u+\Delta V_s)$ gives the second term on the right side of Eq. (4b). Changes in the phase are also conditioned by the mismatch between external wave frequency and resonance frequency (the third term). We should keep in mind that the system (4) was obtained for a soliton and a monochromatic wave propagating in the same direction. For a soliton and a wave propagating in opposite directions the same equations are valid, as long as interaction of counterpropagating perturbations is not taken into consideration. Equations (4) may be obtained also from equations describing soliton excitation by traveling perturbations. This approach was developed, for example, by Sleath.[28] The qualitative analysis of solutions to the system (4) showed that stable steady states for φ_s and amplitude A_s satisfy the relations[23]

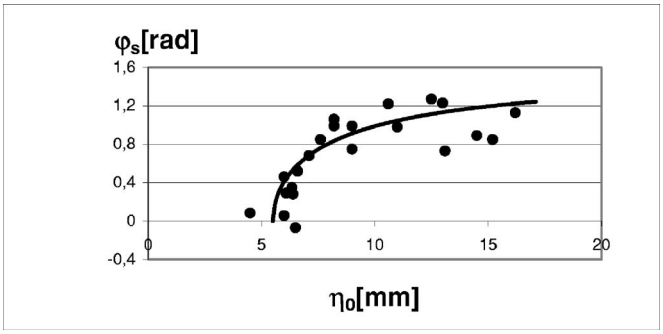

FIG. 11. The soliton phase φ_s *versus* the amplitude η_0 of a harmonic wave (dots), and the theoretical dependence (5a) for $\alpha=0.015$ Hz (curve).

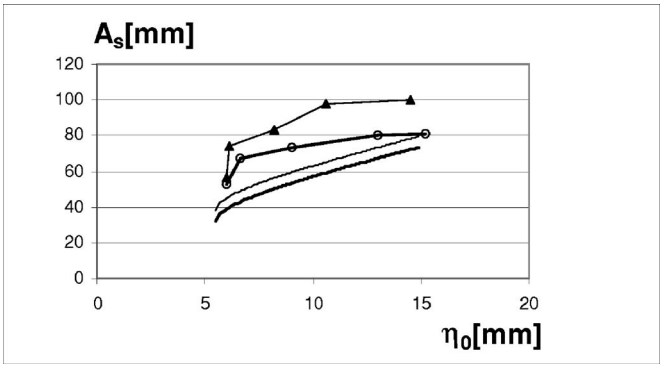

FIG. 12. Soliton amplitude A_s *versus* amplitude η_0 of a harmonic wave: the dots connected by broken curves are for experimental data; solid curves are for the theoretical dependence (5b). The thick curves correspond to mismatch $\Delta=0.063$ rad/s; the thin curves to $\Delta=0.075$ rad/s.

$$\varphi_s = \arccos\left(\frac{2H\alpha}{3\omega\eta_0}\right), \tag{5a}$$

$$A_s = \frac{2\Delta}{k}\sqrt{\frac{H}{g}} + 2\eta_0\sqrt{1-\left(\frac{2H\alpha}{3\omega\eta_0}\right)^2}. \tag{5b}$$

Using the procedure of soliton amplitude and phase extraction described in Sec. III B we have compared experimental data and theoretical predictions. It follows from the theoretical model that soliton phase does not depend on the frequency mismatch. Therefore, we represent phase φ_s as a function of the harmonic wave amplitude η_0 for all the excitation frequencies at which one soliton was observed in an experiment (Fig. 11). The plot φ_s versus frequency f_{ex} for different amplitudes of excitation (Fig. 8) exhibits points scattered over the plane. However, if we plot the same points in new variables (η_0, φ_s), all points (Fig. 11) group in the vicinity of the theoretical curve [Eq. (5a)]. The soliton amplitude A_s *versus* the harmonic wave amplitude is plotted in Fig. 12 for two different excitation frequencies. For the theoretical curves plotted in Figs. 11 and 12 by solid lines, the value of damping was chosen to be $\alpha=0.015$ Hz. The plots show sufficiently good agreement between the experimental data and theoretical predictions. We have observed that the value of the coefficient α taken for the theoretical calculations correlates well with changes in the Q factor of the harmonic wave having frequency f_2 on the resonance curve width. Measurements gave $Q^{-1}\approx 0.02$. If we assume that the damping of the mode with frequency f_2 is the same as that of the soliton, then calculations give the Q factor: $Q^{-1}\approx 0.023$, which is very close to the measured value.

C. Numerical resolution of the modified Boussinesq equations

The KdV equation cannot reproduce all the spatiotemporal properties of the nonlinear waves observed in the hydrodynamic resonator for different parameters of the external forcing. For an explanation of our experimental results, we have made a numerical simulation of one-dimensional Boussinesq equations describing the propagation of waves on shallow water[1,29] and to which we have added small damping terms:

$$\hat{\eta}_\tau + \hat{u}_\xi + \varepsilon(\hat{u}\hat{\eta})_\xi = \tfrac{1}{6}\mu^2\hat{u}_{\xi\xi\xi} + \gamma_1\hat{\eta}_{\xi\xi} - \gamma\hat{\eta}, \tag{6a}$$

$$\hat{u}_\tau + \hat{\eta}_\xi + \varepsilon(\hat{u}\hat{u})_\xi = \tfrac{1}{6}\mu^2\hat{u}_{\xi\xi\tau} + \gamma_1\hat{u}_{\xi\xi} - \gamma\hat{u}. \tag{6b}$$

These equations (6) are written in dimensionless variables: $\hat{\eta}$ is the displacement of free surface $\hat{\eta}=\eta/\varepsilon H$, hereinafter an overcaret denotes dimensionless variables; $\hat{u}=u/\varepsilon H\omega_{ex}$, where u is the velocity taken at the bottom, τ is the time $\tau=t\omega_{ex}$; ξ is the coordinate along the resonator $\xi=x/L$; $\mu=H/L$; ε is the small parameter of asymptotic expansion introduced in Ref. 1. Note that for a constant depth shallow water, the Boussinesq equations can be written in different systems:[29] the depth-mean velocity basis, the bottom variables basis, and the surface variable basis. In our paper, we have preferred the use of the bottom variables basis, which, in the long-wave approximation, is equivalent to the depth-mean velocity basis. We have supplemented the Boussinesq equation by phenomenological terms describing dissipation. The first type of losses (terms with coefficient γ_1) is associated with viscous damping caused by shear stresses; the intensity of this damping increases in proportion to the square of the wavenumber. The second type (terms with coefficient γ) is related to losses in the boundary layer of the surface wave at the bottom. Losses of this type were discussed in Refs. 26 and 27, where it was shown that they are caused by wave scattering at small-scale turbulence. In our experiment such turbulence exists in a boundary layer at the bottom. Measurements of velocity pulsations in the boundary layer by means of a laser Doppler anemometer revealed a high enough intensity of velocity pulsations at a distance of about 1 mm from the bottom. The corresponding value of Reynolds number defined using the velocity in the wave near the bottom is $\mathrm{Re}=1.6\ 10^5$, which lies in the range of a turbulent boundary layer for oscillating flows.[28] The consideration of both kinds of dissipation is very important in our case, as the finite amplitude of nonlinear waves in a resonator depends on the balance of energy supply to the system due to external forcing and energy losses in the system.

For numerical calculations we used the following boundary conditions at $\xi=0$ and $\xi=1$:

$$\frac{\partial \hat{\eta}}{\partial \xi}(\tau, \xi = 0) = 0, \hat{u}(\tau, \xi = 0) = U_0 \sin(2\pi f t), \tag{7a}$$

$$\frac{\partial \hat{\eta}}{\partial \xi}(\tau, \xi = 1) = 0, \ \hat{u}(\tau, \xi = 1) = 0. \tag{7b}$$

We have modeled the action of the wavemaker by a periodically varying horizontal velocity at one resonator end. Numerical resolution of the system of equations (6) was made with the implicit finite-difference scheme realized using the MATLAB5.3 software:

$$\frac{\eta_j^{n+1} - \eta_j^{n-1}}{2\,\Delta\tau} + \frac{u_{j+1}^n - u_{j-1}^n}{2\,\Delta\xi} + \varepsilon u_j^n \frac{\eta_{j+1}^n - \eta_{j-1}^n}{2\,\Delta\tau} + \varepsilon \eta_j^n \frac{u_{j+1}^n - u_{j-1}^n}{2\,\Delta\xi} = \frac{1}{6}\mu^2 \frac{u_{j+2}^n - 2u_{j+1}^n + 2u_{j-1}^n - u_{j-2}^n}{2\,\Delta\xi^3} + \gamma_1 \frac{\eta_{j+1}^{n+1} - 2\eta_j^{n+1} + \eta_{j-1}^{n+1}}{\Delta\xi^2} - \gamma \eta_j^{n+1},$$

$$\frac{u_j^{n+1} - u_j^{n-1}}{2\,\Delta\tau} + \frac{\eta_{j+1}^n - \eta_{j-1}^n}{2\,\Delta\xi} + \varepsilon u_j^n \frac{u_{j+1}^n - u_{j-1}^n}{2\,\Delta\xi} = \frac{\mu^2}{4\,\Delta\tau}\left(\frac{u_{j+1}^{n+1} - 2u_j^{n+1} + u_{j-1}^{n+1}}{\Delta\xi^2} - \frac{u_{j+1}^{n-1} - 2u_j^{n-1} + u_{j-1}^{n-1}}{\Delta\xi^2}\right) + \gamma_1 \frac{u_{j+1}^{n+1} - u_j^{n+1} + u_{j-1}^{n+1}}{\Delta\xi^2} - \gamma u_j^{n+1}.$$

Here $f_j^n = f(\tau_n, \xi_j)$. These equations were used in the inner nodes of the spatial grid, and boundary conditions (7) were written in difference form.

Let us consider results of numerical computations obtained for different parameters. In the first series of experiments we set the frequency independent damping to be equal to zero ($\gamma = 0$) and investigated the dependence of the time series and space-time diagrams on the amplitude and phase of the forcing. Results for the zero initial conditions $\hat{u}(\tau = 0, \xi) = 0$, $\hat{\eta}(\tau = 0, \xi) = 0$ are presented in Fig. 13. For a small amplitude of external forcing $U_0 = 0.05$ (the dimensional amplitude of wavemaker displacement is $a_{1ex} = 0.325$ cm), standing waves are excited in the system. For a larger amplitude $U_0 = 0.5$ ($a_{2ex} = 3.25$ cm), the shape of the nonlinear waves excited in the system depends on the ratio of the external forcing frequency f_{ex} to the resonance frequency f_2. For $f_{ex}^{(1)} = 0.95 f_2 = 0.1563$ Hz, three pulses are observed on the period; for $f_{ex}^{(2)} = 0.98 f_2 = 0.1612$ Hz we have two pulses, and for $f_{ex}^{(3)} = 1.02 f_2 = 0.1678$ Hz, one pulse. These states are similar to those observed in the experiment for the corresponding parameter values of external forcing (Fig. 3, where corresponding dimensional parameters are indicated).

Both numerical computations and experiments have demonstrated multistability and period doubling. The regime of soliton generation depends on initial conditions. For example, under zero initial conditions, one soliton is generated on a wave period; whereas under the initial conditions corresponding to the generation of two solitons on a period, given the same parameters of external forcing, the regime of two-soliton generation proves to be stable. Alternating generation of two or three pulses or one and two pulses is observed in a definite space of the parameters, i.e., the regime where period doubling occurs. Several pulses on a wave period were also obtained in analytical calculations of surface wave excitation in a cuvette[17,30] when waves were excited by horizontal oscillations of the cuvette. Chester[17] and Ockendon *et al.*[30] sought solutions in the form of counterpropagating waves traveling with constant velocity, whereas our numerical calculation showed that wave velocity may be different on different sections of interaction.

In the second series of experiments, we have varied the ratio of the coefficients of frequency-dependent and frequency-independent dissipation. Under the assumption that the dissipation is largely due to frequency-independent losses, e.g., $\gamma_1 = 10^{-4}$, $\gamma = 15\ 10^{-4}$, an oscillating tail component appears on the intervals between solitons (Fig. 14; compare with Fig. 5 for experimental data). This phenomenon can be explained as follows: when the damping is proportional to $\sim k^2$, energy losses at higher harmonics increase with the number of harmonics, and high-frequency oscillations are suppressed. Consequently, the soliton changes smoothly at the periphery. In the case of frequency-independent damping, higher harmonics have a relatively large amplitude and manifest themselves in the time series obtained in numerical experiment.

It is likely that colliding solitons form oscillating tails by a different mechanism. It was demonstrated in Ref. 31 that the allowance for higher-order approximations in the Boussinesq equation as compared to that used in Eq. (6) results in appearance, on soliton collision, of a radiation field that manifests itself as an oscillating tail. Calculations in Ref. 31 were done in the absence of viscosity and external force. We have not yet investigated in numerical simulation the action of viscous forces on an "oscillating tail" arising when higher-order approximations are taken into account.

D. The difference between solitons observed in experiment and ≪theoretical≫ solitons

We are aware that the nonlinear waves we have investigated in this paper may not satisfy the strict theoretical definition of solitons. It is more correct to refer to them as "slowly varying solitary waves" because of the energy input from the harmonic wave and energy dissipation, as it was shown in Sec. III C, their speeds are not conserved through their interaction.

Experiments revealed that solitons of surface waves are excited in a hydrodynamic resonator against the background of a harmonic mode. We focused special attention on the case when one soliton is excited on a period of the harmonic wave. This regime is realized at the external forcing frequencies larger than the resonance frequency, which is clear from the following considerations. At exact resonance, the period of excited oscillations is $T_r = L/V_0$. It takes for the soliton to propagate from one resonator end to the other with the velocity $V_s > V_0$, the time $T_s = L/V_s < T_r$. Thus, a steady-state regime of single soliton excitation can exist for frequencies larger than the resonance frequency and cannot exist at frequencies lower than the resonance one. At frequencies lower

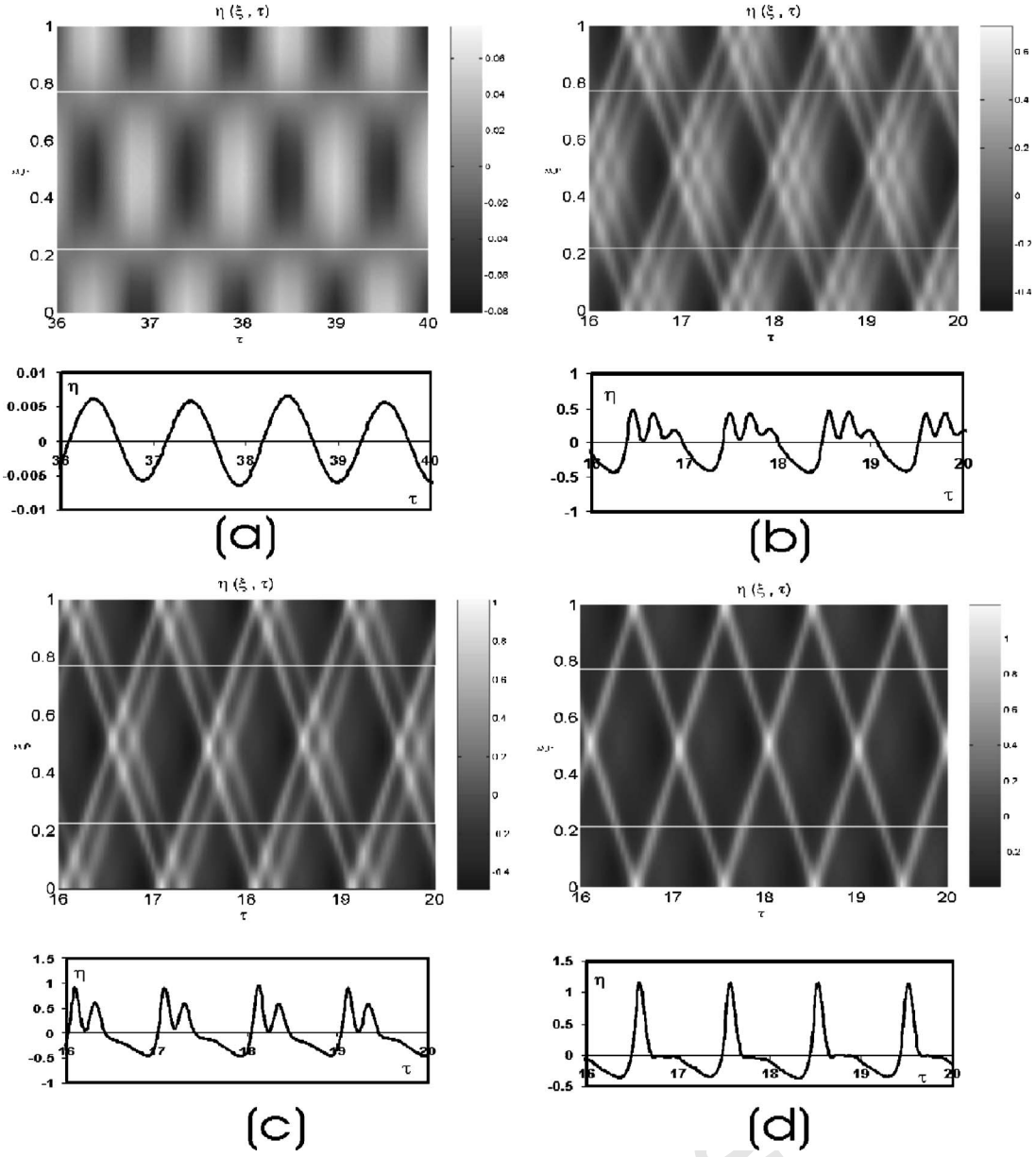

FIG. 13. Results of numerical modeling of the system of Eqs. (6): (a) U_0=0.05 for any frequency f_{ex}; (b) U_0=0.5, f_{ex}=0.95; (c) U_0=0.5, f_{ex}=0.98; (d) U_0=0.5, f_{ex}=1.02. White horizontal lines mark the regions corresponding to the space-time diagrams constructed in the experiment (Fig. 2).

than the resonance frequency, bound states of solitons are excited in a resonator in order to achieve the condition $V_s > V_0$ for an individual soliton. The velocity of these bound states differs from that of a single soliton, and they are excited under different conditions. This is exactly that we observed in experiment.

Our experiment demonstrated that the velocity of soliton propagation in the hydrodynamic resonator is a little smaller than that estimated by the formula (2). For example, for the regime illustrated in Fig. 9, soliton velocity lies in the interval 167 cm/s$< V_s <$173 cm/s. If we estimate V_s by the formula (2) for amplitude A_s=8 cm, which corresponds to the conditions of soliton excitation in the experiment for the data given in Fig. 9, we obtain V_s=184 cm/s (the velocity of waves of infinitely small amplitude is $V_0=\sqrt{gH}$=160 cm/s). How can we explain the discrepancy between the values of velocities obtained theoretically and in experiments? In our opinion two effects should be taken into consideration. First, the soliton is propagating on the background of a harmonic wave. Second, a nonlinear periodic wave (cnoidal wave) rather than a solitary wave is excited in the experiment.

Let us estimate, using the exact solution as a reference one, the difference between the velocities of a soliton and a cnoidal wave. The velocity of a cnoidal wave is known to depend on the so-called elliptic parameter m and is described by the formula[9]

$$V_{cn} = \left[1 - \frac{1}{2}\frac{A_s}{H} + \frac{1}{m}\frac{A_s}{H}\left(1 - \frac{3}{2}\frac{E(m)}{K(m)}\right)\right]\sqrt{gH}, \qquad (8)$$

where $K(m), E(m)$ are complete elliptic functions of the first and second kind. The parameter m (which depends upon the

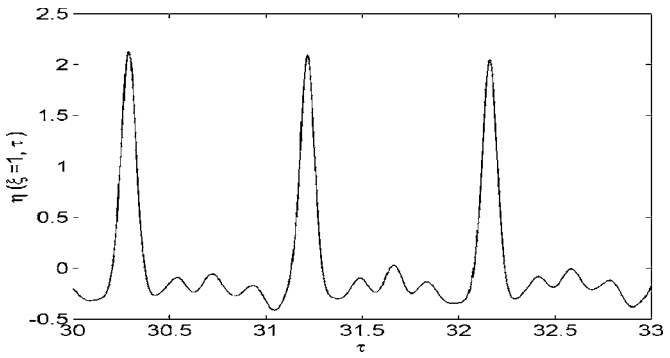

FIG. 14. Solitons with oscillating tails observed in numerical computations for the following parameters: $f_0=1.05$, $V_0=0.5$, $\gamma=1.5\times10^{-3}$, $\gamma_1=10^{-4}$.

ratio of the amplitude to the width of the wave) is responsible for the shape of the wave with $m=0$ corresponding to the harmonic wave, and $m=1$ to the soliton. Using the formula (8), one can estimate the elliptic parameters such that for $A_s=8$ cm and layer depth $H=26$ cm, the propagation velocity should be $V_{cn}=170$ cm/s instead of 184 cm/s, as is given by (2). Estimates from experimental data show that the elliptic parameter for these data is $m=0.9996$, and it differs a little from 1. What are the characteristic features of waves for m close to 1? Let us compare, for instance, cnoidal waves for $m=0.9996$ and $m=0.9999$ (Fig. 15). The shapes of pulses in these two cases are almost indistinguishable, whereas the pulse repetition rates differ appreciably. As $m\to1$, the period tends to infinity, and the propagation velocity differs from the velocity of linear waves on shallow water by a finite value described by the formula (2). For the characterization of cnoidal waves we can introduce quantity $n=T/\tau_s$, where τ_s is the duration of the pulse and T is the period of the cnoidal waves. For the conditions of the experiment we have $n\approx10$, which agrees well with the estimate of the elliptic parameter $m=0.9996$. The estimates presented in this work show that a sequence of solitons and a soliton riding on a harmonic wave have smaller velocities than one soliton without any background. The problem of the velocity of soliton propagation in a resonator needs a further, more detailed investigation. For example, in the interval between solitons, we observed an oscillating component that was not taken into account in the calculations. The velocity of soliton bound states is also an open problem. Although many theoretical and numerical studies on hydrodynamic solitons have been performed,[32] there is still a need for their detailed experimental investigation.

V. CONCLUSION

In this work we have investigated the spatiotemporal properties of solitons excited by harmonic forcing on the surface of a shallow water in a hydrodynamic resonator. We have shown that solitons propagate synchronously with harmonic waves. It was revealed that the solitons are tied up with a definite phase of harmonic wave that depends on the amplitude and frequency of external forcing. We have isolated solitons generated on the background of a harmonic wave and have analyzed their dynamics using space-time

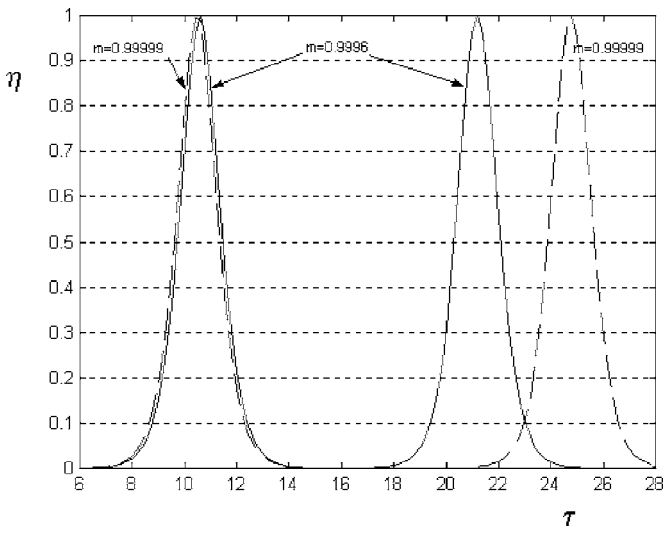

FIG. 15. The shape of cnoidal waves for the values of elliptic parameter close to 1.

diagrams. We have evidenced that the duration of a soliton and the merging length of colliding solitons decrease with the amplitude. We found that there is a small change of velocities of colliding solitons, which may be attributed to a small dissipation of energy due to viscous damping and a turbulent boundary layer. An analytical model of soliton generation based on the amplitude and phase equations was developed and it is consistent with the experimental results. The numerical resolution of the Boussinesq equations with small dissipation terms has provided results that were in good agreement with our experimental data, in particular, for some values of excitation amplitude and frequencies; we have obtained bound states of solitons that require a detailed investigation in the future.

ACKNOWLEDGEMENTS

The authors are grateful to N. Abcha for his assistance and E. Pelinovsky for interesting discussions. This work has been partly accomplished during a PAST position of A.B.E. at Le Havre University with support from the French Ministry of Research. O.Polukhina was supported by INTAS, Project No. N 03-51-3728.

APPENDIX

Let us derive an equation describing changes in the amplitude of a soliton propagating against the background of a harmonic wave. Toward this end, we consider a harmonic wave with frequency Ω and wavenumber χ propagating against the background of a variable flow, the characteristic length of which is much larger than the spatial period of the wave. We assume that $\chi H\ll1$ and regard such a wave as a quasiparticle possessing energy E. Variation of the wave amplitude is caused by energy transfer from a large-scale flow. We estimate the changes in the wave energy E in the reference system moving with the velocity of the large-scale flow in the adiabatic approximation,

$$\frac{\partial}{\partial t}\left(\frac{E}{\Omega}\right)=0. \tag{A1}$$

The frequency Ω depends on the velocity field u and the surface displacement η in a large-scale flow according to

$$\Omega = u\chi + \sqrt{g(H+\eta)}\chi. \tag{A2}$$

If we assume that the large-scale flow is also a wave on shallow water with frequency ω and wave number k, then we have $\Omega \ll \omega$, $kh \ll \chi H \ll 1$. For the short-wave frequency, the relation (A2) reduces to

$$\Omega \approx \eta\sqrt{\frac{g}{H}}\chi + \left(1+\frac{1}{2}\frac{\eta}{H}\right)\sqrt{gH}\chi \approx \frac{3}{2}\eta\sqrt{\frac{g}{H}}\chi + \sqrt{gH}\chi. \tag{A3}$$

Then, from the expressions (A1) and (A2) and using the shallow water condition ($\eta/H \ll 1$), we find the equation

$$\frac{1}{E}\frac{\partial E}{\partial t} = \frac{1}{\Omega}\frac{\partial \Omega}{\partial t} \cong \frac{3}{2H}\frac{\partial \eta}{\partial t}. \tag{A4}$$

Now assume that, instead of a short-wave harmonic wave, we have a cnoidal wave consisting of a set of harmonics. Since the right-hand side of the equation (A4) contains neither the frequency nor the wavenumber of the short wave, the equation (A4) is valid for each harmonic of the cnoidal wave. Then, the cnoidal wave energy $E_{kn}=E_1+E_2+\ldots$, where E_n is the energy of harmonic components, obeys the same equation (A4). The same equation is obtained for the soliton, which is the limiting case of a cnoidal wave. The necessary condition for the energy additivity is that the soliton size should be much smaller than the wavelength of the large-scale wave. Changes in the soliton energy in the reference system moving with velocity ω/k are described by

$$\frac{\partial E_s}{\partial t} = \frac{3}{2}\frac{\omega\eta_0}{H}E_s\cos\varphi_s. \tag{A5}$$

Here, E_s is the soliton energy and φ_s is the phase introduced in Sec. III C. The relation (A5) gives the first term in Eq. (4a). For this equation to describe soliton evolution, it must be supplemented with a term describing energy dissipation [the second term on the right-hand side of (4)]. A similar equation was derived by Gorshkov *et al.*[23] for electromagnetic wave solitons propagating in LC lines.

[1] S. Leibovich and A. R. Seebass, in *Nonlinear Waves* (Cornell University Press, Ithaca, NY, 1974).
[2] M. Remoissenet, *Waves Called Solitons: Concepts and Experiments.* (Springer-Verlag, Heidelberg, 1996). Recent books have been published that address to some extent the hydrodynamic solitons. See, for example E. Infeld and G. Rowlands, *Nonlinear Waves and Solitons and Chaos*, Cambridge University Press, Cambridge, 2000). M. Peyrard and T. Dauxois, *Physique des Solitons* (EDP Sciences, Paris, 2004).
[3] T. Maxworthy, "Experiments on collision between solitary waves," J. Fluid Mech. **76**, 177 (1976).
[4] P. D. Weidman and T. Maxworthy, "Experiments on strong interaction between solitary waves," J. Fluid Mech. **85**, 417 (1978).
[5] A. Bettini, T. A. Minelli, and D. Pascoli, "Solitons in undergraduate laboratory," Am. J. Phys. **51**, 977 (1983).
[6] M. Olsen, H. Smith, and A. C. Scott, "Solitons in a tank," Am. J. Phys. **54**, 826 (1984).
[7] Z. Feng, "Travelling solitary wave solutions to the generalized Boussinesq equation," Wave Motion **37**, 17 (2003).
[8] D. P. Renouard, F. J. Seabra Santos, and A. M. Temperville, "Experimental study of the generation, damping, and reflection of a solitary wave," Dyn. Atmos. Oceans **9**, 341 (1985).
[9] M. J. Cooker, P. D. Weidman, and D. S. Bale, "Reflection of high amplitude wave at a vertical wall," J. Fluid Mech. **342**, 141 (1997).
[10] M. W. Dingemans, *Water Wave Propagation over Uneven Bottoms. Part 2—Non-linear Wave Propagation* (World Scientific, Singapore, 1997).
[11] A. Temperville, "Interaction of solitary waves in shallow water theory. Archives of Mechanics," Arch. Mech. Stosow. **31**, 177 (1979).
[12] M. Oikawa and N. Yajima, "Interactions of solitary waves — a perturbation approach to nonlinear systems," J. Phys. Soc. Jpn. **34**, 1093 (1973).
[13] C. H. Su and R. M. Mirie, "On head-on collision between solitary waves," J. Fluid Mech. **98**, 509 (1980).
[14] H. Power and A. T. Chwang, "On reflection of a planar solitary wave at a vertical wall," Wave Motion **6**, 183 (1984).
[15] J. L. Hammack and H. Segur, "The Korteweg-de-Vries equation and water wave. Part 2. Comparison with experiments," J. Fluid Mech. **60**, 769 (1974).
[16] W. Chester and J. A. Borns, "Resonant oscillations of water waves. II. Experiment," Proc. R. Soc. London, Ser. A **A 306**, 23 (1968).
[17] W. Chester, "Resonant oscillations of water waves. I. Theory," Proc. R. Soc. London, Ser. A **A 306**, 1 (1968).
[18] E. Cox and M. P. Mortell, "The evolution of resonant water-wave oscillations," J. Fluid Mech. **162**, 99 (1986).
[19] H. Ockendon, J. R. Ockendon, and D. D. Waterhouse, "Multi-mode resonances in fluids," J. Fluid Mech. **315**, 317 (1996).
[20] H. Ockendon and J. R. Ockendon, "Nonlinearity in fluid resonances," Meccanica **36**, 297 (2001).
[21] D. Amundsen, E. A. Cox, M. P. Mortell, and S. Reck, "Evolution of nonlinear sloshing in a tank near half the fundamental resonance, Stud. Appl. Math. **107**, 103 (2001).
[22] J. Wu, R. Keolian, and I. Rudnik, "Observation of nonpropagating hydrodynamic soliton," Phys. Rev. Lett. **52**, 1421 (1984); The theoretical explanation of this experiment is given by A. Larraza and S. Putterman, "Theory of non-propagating surface wave soliton," J. Fluid Mech. **148**, 443 (1984).
[23] K. A. Gorshkov., L. A. Ostrovsky, and V. V. Papko, "Parametric amplification and generation of pulses in nonlinear distributed systems (in Russian)," Izv. Vyssh. Uchebn. Zaved., Radiofiz. **16**, 1195 (1973); This research work was also described by L. A. Ostrovsky and A. I. Potapov, in the book *Modulated Waves. Theory and Applications* (The Johns Hopkins Univ. Press, Baltimore, 1999).
[24] A. I. Potapov and A. I. Vesnitsky, "Interaction of solitary waves under head-on collisions Experimental investigation," Wave Motion **19**, 29 (1994).
[25] L. D. Landau and E. M. Lifchitz, *Mécanique des Fluides* (Editions Mir, Moscou, 1990).
[26] R. Grimshaw, E. N. Pelinovsky, and T. G. Talipova, "Damping of large-amplitude solitary waves," Wave Motion **37**, 351 (2003).
[27] L. A. Ostrovsky and I. A. Soustova, "Upper mixed layer of the ocean as a source of energy sink for internal waves (in Russian)," Okeanologiya **XIX**, 973 (1979).
[28] J. F. A. Sleath, *Sea Bed Mechanics* (Wiley, Chichester, 1984).
[29] J. E. Zhang, C. Chen, and Y. Li, "On Boussinesq models of constant depth," Phys. Fluids **16**, 1287 (2004).
[30] H. Ockendon, J. R. Ockendon, and A. D. Johnson, "Resonant sloshing in shallow water," J. Fluid Mech. **167**, 465 (1986).
[31] J. G. B. Byatt-Smyth, "The reflection of a solitary wave by a vertical wall," J. Fluid Mech. **197**, 503 (1988).
[32] G. Iooss and F. Dias, "Water-waves as a spatial dynamical system," in *Handbook of Mathematical Fluid Dynamics*, edited by S. Friedlander and D. Serre, Elsevier Science B.V., Amsterdam, 2003), Vol. 2, pp. 443-499.

AQ: #1
AQ: #2
AQ: #3

AUTHOR QUERIES — 036605PHF

#1 Author: there is no Eq. 4.1. Please check
#2 Author: please check year; doesn't match journal years of publication
#3 Author: please supply journal coden, Ref. 27